Supporting Information

A General Approach to the Evolution of Singlet Nanoparticles from a Rapidly-quenched Point Source

Jicheng Feng, [a] *Luyi Huang,* [a] *Linus Ludvigsson,* [b] *Maria E. Messing,*[b] *Anne Maisser,*[a, c] *George Biskos,*[a, d, e] *and Andreas Schmidt-Ott,*[a,*]

[a]Faculty of Applied Science, Delft University of Technology, 2628 BL, The Netherlands

[b]Solid State Physics, Lund University, S-22100, Sweden

[c]Department of Mechanical Engineering, University of Minnesota, Minneapolis, 55455 MN, USA

[d]Faculty of Civil Engineering and Geosciences, Delft University of Technology, 2628 CN, Delft, The Netherlands

[e]Energy Environment and Water Research Centre, The Cyprus Institute, 2121 Nicosia, Cyprus

*to whom correspondence should be addressed to: a.schmidt-ott@tudelft.nl

Section S1 Estimation of the vapor cloud supersaturation

Quantitative prediction for the critical nucleus size is often not possible as the data for supersaturation and surface tension are not well known. The surface tension of these NPs are directly used from the literatures,[1–3] whereas the supersaturation is approximated by equation (S1) further below.

The supersaturation S can be approximated as:

$$S = \frac{p_\mathrm{a}}{p_\mathrm{s}} \quad \text{(S1)}$$

where p_a and p_s are the actual pressure and saturated pressure, respectively.

The saturated pressure can be determined from Clausius–Clapeyron equation assuming that the enthalpy of vaporisation H_v is independent of temperature given by:

$$p_\mathrm{s} = p_0 \exp\left(\frac{H_\mathrm{v}}{R}\left(\frac{1}{T_\mathrm{b}} - \frac{1}{T_\mathrm{c}}\right)\right) \quad \text{(S2)}$$

where p_0 is the atmospheric pressure, T_b the boiling temperature, R is universal gas constant, and T_c is the room temperature.

Assuming the ideal gas law for the vapor cloud, p_a can be estimated as:

$$p_\mathrm{a} = N_0 k T_\mathrm{c} \quad \text{(S3)}$$

Where k is the Boltzmann constant and N_0 is the initial number concentration, which is in the order of 10^{20} m^{-3}.

The critical nucleus size d^* can be derived from Kelvin equation:

$$d^* = \frac{4\gamma_s \Omega}{kT_c \ln(S)} \qquad \text{(S4)}$$

where Ω is the atomic volume and γ_s is the surface tension.

Taking the examples Au and Ag, the supersaturation and critical nucleus sizes are shown in Table S1. Values of their physical properties are provided in Table S2 and S3 further below.

Table S1 The supersaturation and critical nucleus size for Au and Ag

	Au	Ag
S	1.24×10^{50}	2.86×10^{34}
d^* (nm)	0.86	0.85~1.03

Section S2 Material properties and constants

Based on the energy balance, the mass of the produced vapor can be expressed as a function of the energy per spark E as follows:[4]

$$\Delta m = \frac{\alpha E - 2\pi r^2 \sigma \tau (T_b^4 - T_c^4) - 2\pi r \tau k_e (T_b - T_c) - 2\pi r \tau k_a (T_b - T_c)}{c_{ps}(T_m - T_c) + c_{pl}(T_b - T_m) + H_m + H_e} \qquad \text{(S5)}$$

Here α is the fraction of spark energy consumed for NP production, c_{ps} and c_{pl} (J K^{-1} kg^{-1}) the heat capacities of the solid and liquid material, τ (s) the spark duration, r (m) the radius of the spark channel, k_e and k_a (W m^{-1} K^{-1}) the thermal conductivity of the electrode material and carrier gas, respectively, T_c, T_b, and T_m (K) the temperatures of the carrier gas, the boiling and melting points of the electrode materials, respectively, H_m and H_e (J kg^{-1}) are the enthalpies of melting and vaporization of electrode materials, and σ (5.67×10^{-8} W m^{-2} K^{-4}) is the Stefan–Boltzmann constant.

The constant portion of spark energy α = 0.18% has been empirically determined by gravimetric measurement for all gap distances (see Section S6).

Table S2 Constants used in the calculations

Stefan–Boltzmann constant	$\sigma = 5.67\times10^{-8}$ W m^{-2} K^{-4}
Avogadro constant	$N_A = 6.02\times10^{23}$ mol^{-1}
Boltzmann constant	$k = 1.38\times10^{-23}$ J K^{-1}
Universal gas constant	$R = 8.31$ J K^{-1} mol^{-1}
Material-dependent constant C in equation (1)	$\frac{\alpha}{c_{ps}(T_m - T) + c_{pl}(T_b - T_m) + H_m + H_e}$
The threshold energy E_0 to produce NPs in equation (1)	$\frac{2\pi r^2\sigma\tau(T_b^4 - T^4) + 2\pi r\tau k_e(T_b - T) + 2\pi r\tau k_a(T_b - T)}{\alpha}$

Table S3 Material properties at atmospheric conditions

Material properties	symbol	Au	Ag
Surface tension	γ_s (N m^{-1})	8.78[1]	5.9~7.20[2,5]
Heat capacities of the solid	c_{ps} (J K^{-1} kg^{-1})	129	235
and liquid materials	c_{pl} (J K^{-1} kg^{-1})	129	235
Thermal conductivity	k_e (W m^{-1} K^{-1})	318	429
Boiling point	T_b (K)	3243	2435
Melting point	T_m (K)	1337	1235
Enthalpies of melting	H_m (J kg^{-1})	6.37×10^4	1.04×10^5
Enthalpies of vaporizing	H_e (J kg^{-1})	1.74×10^6	2.35×10^6
	H_v (J mol^{-1})	3.42×10^5	2.54×10^5
Molar weight	M (Kg mol^{-1})	0.197	0.108
Atom diameter	d_a (nm)	0.288	0.288
	N_2		
Thermal conductivity	k_a (W m^{-1} K^{-1})	25.83×10^{-3}	
Temperature	T_c (K)	293	
Dynamic viscosity	μ (Kg m^{-1} s^{-1})	1.75×10^{-5}	
Mean free path	λ (nm)	58.80	

Table S4 Characteristics of the sparks

Energy per spark	E = 0.15 ~ 180 mJ
Spark duration	τ = 1.2 μs
Radius of the spark channel	r = 1.5 μm

Section S3 Independence of the portion of the spark energy on gap distances

Based on the energy balance, the mass of the vapor can be expressed as a function of energy per spark given by equation (S5).[4]

Using the constants provided in Tables S2, S3 and S4 and equation (S5), the value of the individual terms, namely radiation, metallic thermal condition as well as convection and conduction in the gas, for Au and Ag are summarized in Table S5.

Table S5 Energy consumed to a hot-spot consumed by radiation, metallic thermal conduction, and convection and conduction in the gas

Terms	Au (J)	Ag (J)
Radiation: $2\pi r^2\sigma\tau(T_b^4 - T_c^4)$	1.06×10^{-10}	3.38×10^{-11}
Electrode thermal conduction: $2\pi r\tau k_e(T_b - T_c)$	1.06×10^{-5}	1.04×10^{-5}
Convection and conduction in the gas: $2\pi r\tau k_a(T_b - T_c)$	8.62×10^{-10}	6.26×10^{-10}

Table S5 shows that the metallic conduction contrasting to radiation and convection in the gas, is largely dominate in equation (S5). This finding suggests that the electrode gap distance is independent of the portion of spark energy (i.e., α in equation. (S5)) consumed for NP production. In the case of larger distance, the spark energy distributes over a larger volume where the radiation is emitted.[6] However, radiation is only 0.001 % of metallic conduction. On the contrary, changes of the gap distance do influence the passing gas flow conditions and lead to different efficiency of material transportation. The thermal conduction of Au and Ag is similar as shown in Table S3. Therefore, constant α probably validates for all the gap distances. The other processes, for instance, the energy absorbed as heat by evaporation of electrons (cathode) and positive ions (anode) can also affect α.

Section S4 Fuchs form of the coagulation kernel

Table S6 Fuchs form of the Coagulation Kernel β

Coagulation Kernel[7]	$\beta = 8\pi\epsilon\varphi D d_{\mathrm{p}} \left(\frac{d_{\mathrm{p}}}{d_{\mathrm{p}} + g} + \frac{8\theta D}{c_{\mathrm{p}} d_{\mathrm{p}}} \right)^{-1}$
Diffusion coefficient[8]	$D = \frac{k T_{\mathrm{c}} C_{\mathrm{c}}}{3\pi\mu d_{\mathrm{p}}}$
Cunningham slip correction factor[8]	$C_{\mathrm{c}} = 1 + \frac{\lambda}{d_{\mathrm{p}}}(2.34 + 1.05\exp(-0.39\frac{d_{\mathrm{p}}}{\lambda})$
Particle velocity [7]	$c_{\mathrm{p}} = (\frac{48 k T_{\mathrm{c}}}{\pi^2 \rho d_{\mathrm{p}}^3})^{1/2}$
Transition parameter [7]	$g = \frac{1}{3 d_{\mathrm{p}} l}[(d_{\mathrm{p}} + l)^3 - (d_p{}^2 + l^2)^{3/2}] - d_{\mathrm{p}}$ $l = \frac{8D}{\pi c_{\mathrm{p}}}$
Enhancement factor by van der Waal forces[9,10]	$\varepsilon \approx 3$ for size ca. 5 nm from reference[10]
Enhancement factor by poly-dispersity[11]	$\varphi = \frac{3\sqrt{3}}{2} b \left(\frac{\mu^2 d_{\mathrm{p}}}{\rho k T_{\mathrm{c}}} \right)^{1/2} \left[\exp\left(\frac{25}{8} ln^2\sigma \right) + 2\exp\left(\frac{5}{8} ln^2\sigma \right) + \exp\left(\frac{1}{8} ln^2\sigma \right) \right]$ b ranges from $\frac{1}{\sqrt{2}}$ for σ =1.0 to 0.8755 for σ =3.0
Sticking probability[7]	$\theta = 1$

Section S5 Comparison between the predicted and measured mean diameter of Ag NPs

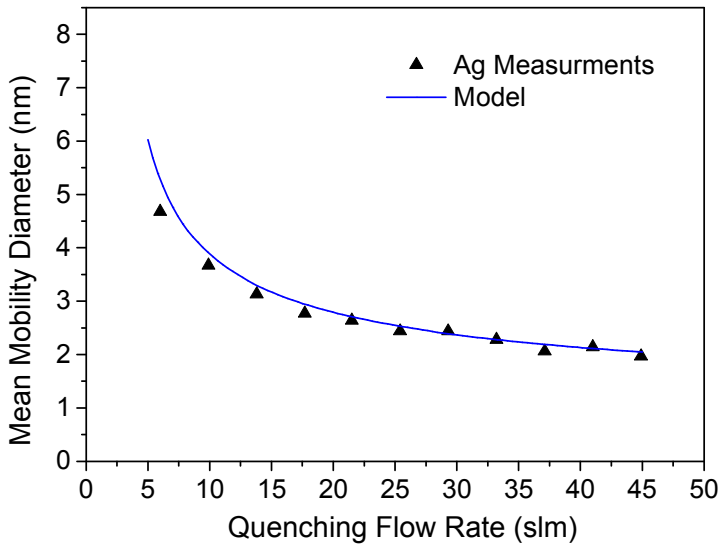

Fig. S1 Measured and predicted geometric mean diameter of Ag singlet particles as a function of quenching gas flow rate.

Fig. S1 shows a comparison between measured and predicted Ag particles as a function of quenching gas flow rate and provides the evidence to generalize our model to other materials, e.g., Ag, while main manuscript uses Au particles (cf. Fig. 4). For the predictions in Fig. S1, we used the same system parameters as for Au, with the only exception of the η in equation. (15) in the main manuscript, which was 0.715 instead of 0.75.

Section S6 Proximity collection of the early stage clusters

To verify our assumption 1) in the main manuscript and compare the volume of initial vapor cloud to the model, we collected NPs close to the spark by a Mini-Particle Sampler (MPS),[12] which carries a TEM grid with holes, through which the aerosol flow passes. Particle collection can thus be described as a filtration process.

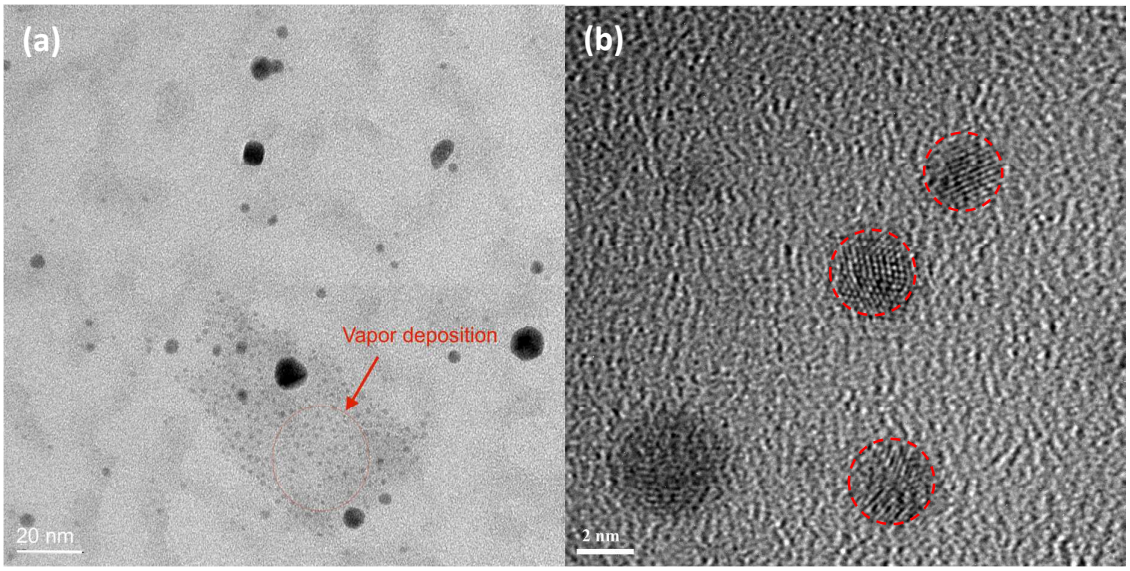

Fig. S2 TEM images Au NPs collected at a distance of ca. 8 mm downstream of the spark with different scale bar, (a) 20 nm and (b) 2 nm.

Fig. S2 shows TEM image of MPS sampled NPs close to the spark (cf. a distance of ca. 8 mm from spark, which is in range of our model prediction for the initial vapor cloud volume) and the grey areas seems to be a deposited film, which indicates the TEM grid is positioned in the vapor domain. Because thin films or very small particles are liquid-like at room temperature, surface tension leads to the formation of patches, within which small droplets form, similar to what happens with a water film on glass. In the area indicated of Fig. S2a by the solid circle, enough material has accumulated for these droplets to grow to a size between 1 and 2 nm, and become visible in TEM. The micrograph thus indicates that the depositing species are smaller than 1 nm (vapor atoms or small clusters). Thus at the distance of ca. 8 mm from the spark (i.e., the vapor from a 1 mm gap having flow rate of 10 slm needs ca. 0.4 ms to reach TEM grid), the plume is still in a vapor-like state. The estimated quenching rate from boiling point to room temperature during 0.4 ms is 7.5×10^6 K s^{-1}, which agrees to the literatures ($10^6 \sim 10^9$ K s^{-1}).[13–15] The micrograph thus justifies the assumption 1) that the cooling time from the boiling point to the carrier gas temperature T_c (usually room temperature) is so short that the

starting condition in Stages *B* and *C* (i.e., the entire spark chamber) is a vapor at T_c, and collisional growth occurs under this constant temperature T_c throughout the system. The large particles (i.e., a few nm in size) shown in Fig. S2a are due to the recirculation of the aerosol in the particle generator.

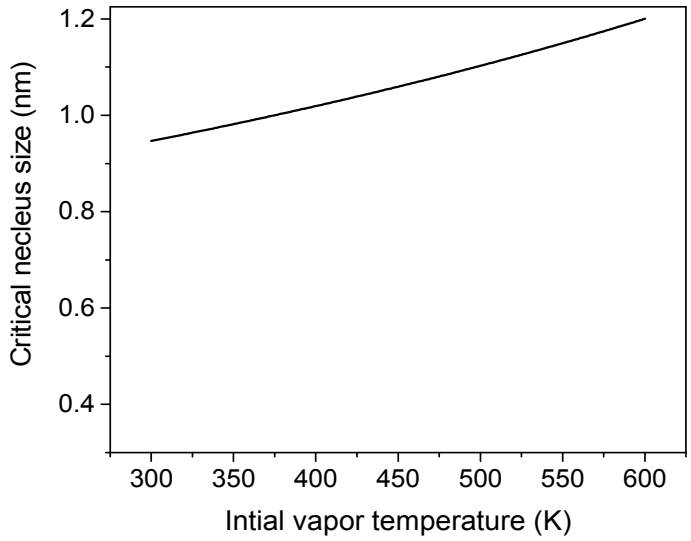

Fig. S3. Dependence of the vapor temperature on the critical nucleus size.

Due to very short spark duration (<10 μs), the temperature downstream of the discharge, where the TEM grid is located (ca. 8 mm away from the spark) hardly exceeds room temperature. Multiple crystalline domains within the sampled NPs are observed by HRTEM images (cf. Fig. S2b). This observation confirms that the temperature downstream of the spark stays low. Otherwise, in-flight collisions of hot, newly-formed clusters would lead to full epitaxial crystallization, assisted by the high temperature. Grammatikopoulos et al. also reported that multiple domains will be formed if the NPs coalesce at room temperature.[16] Sparks or laser ablation configurations with a higher energy per pulse or a higher repetition frequency than the one we used would still fulfill this condition of "rapid quenching" when the gas flow rate is increased accordingly. In addition, our earlier work showed that assuming single atoms in the initial state does not have to be fulfilled in a strict sense, as the final particle size is insensitive to the initial one at a given mass loading.[17] This means that even if

quenching is not drastic enough to disable classical nucleation, our simple assumption of a vapor condensing at room temperature leads to correct results (cf. Figures 4 and 7 in the main manuscript).

Section S7 Laminar deposition rate K_{df2}

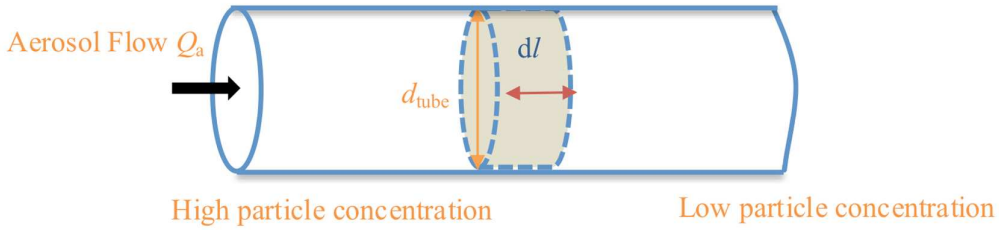

Fig. S4 Schematic diagram of a circular tube. The aerosol NPs pass through this tube and a differential variable in it is used to estimate the diffusional loss rate under laminar flow conditions.

Diffusion of aerosol particles on the walls leads to a concentration gradient from left to right through a circular tube with a length of dl. The number of particles dn deposited per unit area of surface during a time dt is given by:[8]

$$\mathrm{d}n = N_0 \left(\frac{D}{\pi t}\right)^{1/2} \mathrm{d}t \qquad \text{(S6)}$$

For a tube with the diameter d_{tube} and the length of dl during time dt, the total number of deposited particles Σ onto the walls can be expressed as:

$$\Sigma = \pi d_{tube}\, \mathrm{d}l\, \mathrm{d}n \qquad \text{(S7)}$$

Under laminar flow conditions, the concentration decay by diffusional losses can be described by:[8]

$$\mathrm{d}N = -K_{df2} N \mathrm{d}t \qquad \text{(S8)}$$

In this case, Σ can be calculated by:

$$\Sigma = -\frac{\pi}{4} {d_{\mathrm{tube}}}^2 \mathrm{d}l \, \mathrm{d}N \tag{S9}$$

Combining equations (S6)-(S9), we arrive at:

$$\Sigma = \pi d_{\mathrm{tube}} \, \mathrm{d}l \, N_0 \, (\frac{D}{\pi t})^{1/2} \mathrm{d}t = \, -\frac{\pi}{4} {d_{\mathrm{tube}}}^2 \, \mathrm{d}l \, (-K_{\mathrm{df2}} N \, \mathrm{d}t) \tag{S10}$$

Equation (S10) can be simplified to:

$$\frac{4 \, (\frac{D}{\pi t})^{1/2}}{d_{\mathrm{tube}}} = K_{\mathrm{df2}} \frac{N}{N_0} \tag{S11}$$

Integrating equation (S8), the penetration is given by:

$$P = \frac{N}{N_0} = \exp(-K_{\mathrm{df2}} t) \tag{S12}$$

Combining equation (S11) and (S12), the laminar deposition rate can be implicitly expressed as:

$$K_{\mathrm{df2}} \, = \exp(K_{\mathrm{df2}} t) \frac{4 \, (\frac{D}{\pi t})^{1/2}}{d_{\mathrm{tube}}} \tag{S13}$$

Equation (S13) can also be rewritten by replacing $t = \frac{\pi {d_{\mathrm{tube}}}^2 L}{4 Q_{\mathrm{a}}}$ as:

$$K_{\mathrm{df2}} \, = \exp(K_{\mathrm{df2}} \frac{\pi {d_{\mathrm{tube}}}^2 L}{4 Q_{\mathrm{a}}}) \frac{2 \, \pi (\frac{D Q_{\mathrm{a}}}{L})^{1/2}}{{d_{\mathrm{tube}}}^2} \tag{S14}$$

Section S8 Size evolution of particles

The procedures of size evolution for other stages based on the mass conservation are analogous to Stage *B* where turbulent dilution and coagulation occur, because the reduction of

NP mass in per unit volume is only driven by dilution or diffusion. Here we only use Stage *B* as an example to describe the procedures to get the geometric mean size evolution of the particles. The concentration decay rate in Stage *B* can be described as:

$$\frac{\mathrm{d}N}{\mathrm{d}t} = -\frac{1}{2}\beta N^2 - K_{\mathrm{dl}}N \qquad (t \le t_{\mathrm{B}}) \quad \text{(S15)}$$

In order to use the mass conservation, the diameter of the particle with average mass $d_{\overline{\mathrm{m}}}$, however, must be converted from the geometric mean diameter d_{p} by Hatch-Choate conversion equation given by:

$$d_{\overline{\mathrm{m}}} = d_{\mathrm{p}} \exp(1.5 \ln^2 \sigma_{\mathrm{g}}) \qquad \text{(S16)}$$

where σ_{g} is the geometric standard deviation and can be regarded as a self-preserving value of 1.35. Therefore, the conversion factor is a constant and it is generally valid for any log-normal size distribution.

In Stage *B*, the NP mass in per unit volume is reduced only by dilution so the reduction rate can be expressed as:

$$\frac{\mathrm{d}\left(\rho\frac{\pi}{6}(\exp(1.5 \ln^2 \sigma_{\mathrm{g}})d_{\mathrm{p}})^3 N\right)}{\mathrm{d}t} = -K_{\mathrm{dl}}\,\rho\frac{\pi}{6}(\exp(1.5 \ln^2 \sigma_{\mathrm{g}})d_{\mathrm{p}})^3 N \;\; (t \le t_{\mathrm{B}}) \quad \text{(S17)}$$

Cancelling out the constants on both sides of equation (S17), it is thus simplified to:

$$\frac{3d_{\mathrm{p}}^2 N\mathrm{d}(d_{\mathrm{p}}) + d_{\mathrm{p}}^3 \mathrm{d}N}{\mathrm{d}t} = -K_{\mathrm{dl}}\,{d_{\mathrm{p}}}^3 N \qquad (t \le t_{\mathrm{B}}) \qquad \text{(S18)}$$

Substituting equation (S15) in equation (S18), we finally obtain the mean size evolution:

$$\frac{\mathrm{d}d_{\mathrm{p}}}{\mathrm{d}t} = \frac{1}{6}\beta N d_{\mathrm{p}} \qquad \text{(S19)}$$

Section S9 Relation between volume and mass of initial vapor cloud

After the vapor produced by the point source, it has adiabatically expanded to ambient pressure p_0, and reached a temperature T_A. Its thermal energy E_{th}, a fixed fraction of the spark energy E, is proportional to nT_A ($E_{th} \propto nT_A$), where n is the number of moles. Applying the ideal gas law to this vapor cloud leads to $E_{th} \propto p_0 V_A$, which means that V_A is proportional to the spark energy E and thus approximately to the mass per spark, Δm, considering equation (S5) and Fig. 4. The vapor cloud is subsequently cooled and diluted by mixing with the quenching gas (room temperature T_c). Cooling to a given temperature T_S means expansion of V_A by a given factor to V_o, which we call initial volume, as it marks the starting point of our coagulation model. These considerations are in line with a value of $\eta = 0.75$ close to 1. Note that in practise T_S is close to T_C, and we have assumed coagulation at the quenching gas temperature.

Section S10 Estimation of the penetration

In contrast to Gormley-Kennedy theory,[18] the elegance of our method to estimate the penetration through a circular tube lies in the simplicity of calculating K_{df2} (cf. equation (S14)). Since the residence time is always easy to calculate, one can easily use equations (S12) and (S14) to estimate the penetration for any geometry. The penetration predicted by Gormley-Kennedy theory, is comparable to that predicted using equations (S12) and (S14) (cf. Fig. S5).

Fig. S5 compares the penetration predicted by equation (S8) and Gormley-Kennedy model as a function of deposition parameter ($\xi = \frac{DL}{Q_a}$) for circular tubes with a length L. The points in Fig. S5 are chosen in a laminar circular tube with an inside diameter of 4 mm and length of 40 mm. The residence time is 0.181 s based on an aerosol flow rate Q_a = 1.67 slm and the

dimensions of this circular tube. For easy calculations, we do not consider particle growth in this short time. Briefly, we calculate penetration by equation (S12), where K_{df2} is estimated by equation (S14) for one particle size.

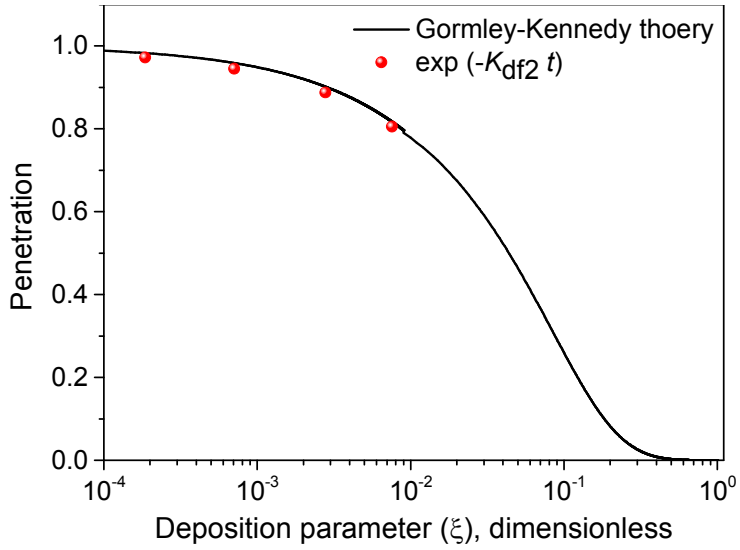

Fig. S5 Penetration versus deposition parameter for circular tubes and the comparison between Gormley-Kennedy theory and our method (cf. using equations (S12) and (S14)).

References in the Supporting Information

(1) Nanda, K. K.; Maisels, A.; Kruis, F. E. Surface Tension and Sintering of Free Gold Nanoparticles. *J. Phys. Chem. C* **2008**, *112*, 13488–13491.

(2) Nanda, K. K.; Maisels, A.; Kruis, F. E.; Fissan, H.; Stappert, S. Higher Surface Energy of Free Nanoparticles. *Phys. Rev. Lett.* **2003**, *91*, 106102.

(3) Vanithakumari, S. C.; Nanda, K. K. Phenomenological Predictions of Cohesive Energy and Structural Transition of Nanoparticles. *J. Phys. Chem. B* **2006**, *110*, 1033–1037.

(4) Llewellyn Jones, F. Electrode Erosion by Spark Discharges. *Br. J. Appl. Phys.* **1950**, *1*, 60–65.

(5) Hofmeister, H.; Thiel, S.; Dubiel, M.; Schurig, E. Synthesis of Nanosized Silver Particles in Ion-Exchanged Glass by Electron Beam Irradiation. *Appl. Phys. Lett.* **1997**, *70*, 1694.

(6) Tabrizi, N. S.; Ullmann, M.; Vons, V. A.; Lafont, U.; Schmidt-Ott, A. Generation of Nanoparticles by Spark Discharge. *J. Nanoparticle Res.* **2009**, *11*, 315–332.

(7) Seinfeld, J. H.; Pandis, S. N. *Atmospheric Chemistry and Physics: From Air Pollution to Climate Change*; John Wiley & Sons: New York, 2006.

(8) Hinds, W. C. *Aerosol Technology: Properties, Behavior, and Measurement of Airborne Particles*; John Wiley & Sons: New York, 1999.

(9) Marlow, W. H. Size Effects in Aerosol Particle Interactions: The Van Der Waals Potential and Collision Rates. *Surf. Sci.* **1981**, *106*, 529–537.

(10) Kennedy, I. M.; Harris, S. J. Direct Numerical Simulation of Aerosol Coagulation with van Der Waals Forces. *J. Colloid Interface Sci.* **1989**, *130*, 489–497.

(11) Lee, K. W.; Chen, H. Coagulation Rate of Polydisperse Particles. *Aerosol Sci. Technol.* **1984**, *3*, 327–334.

(12) R'mili, B.; Le Bihan, O. L. C.; Dutouquet, C.; Aguerre-Charriol, O.; Frejafon, E. Particle Sampling by TEM Grid Filtration. *Aerosol Sci. Technol.* **2013**, *47*, 767–775.

(13) Martinen, H.; Tholl, H. Untersuchung Der Temperatur Und Der Expansion von Funkenkanälen in H2 Bei Variabler Energiezufuhr. *Zeitschrift für Naturforsch. A* **1970**, *25*, 430–439.

(14) Jenkins, N. T.; Eagar, T. W. Submicron Particle Chemistry: Vapor Condensation Analogous to Liquid Solidification. *JOM* **2003**, *55*, 44–47.

(15) Berkowitz, A. E.; Walter, J. L. Spark Erosion: A Method for Producing Rapidly Quenched Fine Powders. *J. Mater. Res.* **1987**, *2*, 277–288.

(16) Grammatikopoulos, P.; Cassidy, C.; Singh, V.; Sowwan, M. Coalescence-Induced Crystallisation Wave in Pd Nanoparticles. *Sci. Rep.* **2014**, *4*, 5779.

(17) Feng, J.; Biskos, G.; Schmidt-Ott, A. Toward Industrial Scale Synthesis of Ultrapure Singlet Nanoparticles with Controllable Sizes in a Continuous Gas-Phase Process. *Sci. Rep.* **2015**, *5*, 15788.

(18) Ingham, D. B. Diffusion of Aerosols from a Stream Flowing through a Cylindrical Tube. *J. Aerosol Sci.* **1975**, *6*, 125–132.